

# Molecular Design of Interfacial Modifiers for Polymer-Inorganic Hybrid Solar Cells

Jusfong Yu, Tsung-Lung Shen, Wei-Hsiang Weng, Yu-Chen Huang, Ching-I Huang,\*  
Wei-Fang Su, Syang-Peng Rwei, Kuo-Chuan Ho, and Leeyih Wang\*

The heterojunction of poly(3-hexylthiophene) (P3HT) and TiO<sub>2</sub> in hybrid solar cells is systematically engineered with four cyanoacrylic acid-containing conjugated molecules with various lowest unoccupied molecular orbital (LUMO) levels, WL-1 to WL-4, which are prepared by the formylation of thiophene derivatives in a Vilsmeier–Haack reaction, followed by treatment with cyanoacetic acid. The optical characteristics, redox properties, and intrinsic dipole moments of these interfacial modifiers (IMs) are examined using UV-vis spectrophotometry, cyclic voltammetry, and density functional theory calculations. Using cyanoacrylic acid as a terminal anchoring group in IMs increases the electron affinity in regions close to the titania surface and forms a molecular dipole that is orientated away from the TiO<sub>2</sub> surface, enabling both open-circuit voltage ( $V_{OC}$ ) and short-circuit current density to be increased simultaneously. Photovoltaic measurements demonstrate that  $V_{OC}$  increases with the dipole moment of IMs along the molecular backbone. Moreover, the external quantum efficiency (EQE) spectra display a bimodal distribution, revealing that both IMs and P3HT contribute to the photocurrent. The EQE at 570 nm is identified as characteristic of P3HT. More importantly, the LUMO of the IMs decisively determines the dissociation efficiency of P3HT excitons. The device based on P3HT/WL-4/TiO<sub>2</sub> exhibits the highest power conversion efficiency of 2.87%.

low-cost photovoltaic cells.<sup>[1–3]</sup> Recent efforts have demonstrated the feasibility of polymer solar cells using fullerene derivatives<sup>[4,5]</sup> as acceptor combination with a polymer acting as a donor, leading to encouraging efficiencies of 7%–8%.<sup>[6,7]</sup> Alternatively, other works have devised hybrid solar cells based on conjugated polymers combined with *n*-type inorganic semiconductors, including CdSe,<sup>[8–10]</sup> TiO<sub>2</sub>,<sup>[11–13]</sup> and ZnO,<sup>[14,15]</sup> owing to the high electron mobility and excellent chemical and physical stability of inorganic semiconductors.<sup>[16,17]</sup> Among them, TiO<sub>2</sub> has been widely used as an acceptor to fabricate hybrid cells because of its reputation as a safe, environmentally stable, and inexpensive material. However, polymer-TiO<sub>2</sub> hybrid solar cells described in recent years had relatively low efficiencies (<0.5%).<sup>[18,19]</sup> Of priority concern, the *p*-type polymers and *n*-type semiconductors used in hybrid solar cells commonly have a poor compatibility, resulting in serious charge recombination at the donor–acceptor interface.<sup>[20,21]</sup> Recently, Chen and co-workers<sup>[22]</sup> modified the surface of titania nanorods with a

monolayer of interfacial modifiers (IMs), capable of increasing the compatibility of poly(3-hexylthiophene) (P3HT) and TiO<sub>2</sub>, as well as suppressing back recombination, ultimately leading to a substantial increment in cell efficiency to 1.12%–2.20%. Very recently, close contact of polymer chains with titania surface was also achieved by functionalization of both chain ends of P3HT with cyanoacetic groups that markedly increases the charge injection efficiency, subsequently producing a power conversion efficiency of 2.2%.<sup>[23]</sup>

Many studies have also demonstrated that the formation of a self-assembled monolayer of IM on the surface of inorganic semiconductors or metals that produces an interfacial dipolar layer can adjust the work function of substrate materials.<sup>[24,25]</sup> The change in work function is ascribed to the redistribution of electrons by charge transfer and hybridization of wave functions of the organic molecules and substrate surface.<sup>[26,27]</sup> An IM with a dipole pointing away from the substrate, in which the dipole direction is defined from negative pole toward positive pole, induces a vacuum level raise across this dipolar interfacial layer to the substrate surface that upshifts the work function of substrate, as shown in **Figure 1a**; meanwhile, an IM with a

## 1. Introduction

Organic solar cells based on conjugated polymers have attracted considerable interest in recent decades owing to their great potential for fabricating large-area, physically flexible, and

J. Yu, T.-L. Shen, W.-H. Weng, Y.-C. Huang, Prof. C.-I. Huang,  
Prof. W.-F. Su, Prof. K.-C. Ho, Prof. L. Wang  
Institute of Polymer Science and Engineering  
National Taiwan University  
Taipei 106, Taiwan  
E-mail: chingih@ntu.edu.tw; leewang@ntu.edu.tw

Prof. S.-P. Rwei  
Institute of Organic and Polymeric Materials  
National Taipei University of Technology  
Taipei 106, Taiwan

Prof. L. Wang  
Center for Condensed Matter Sciences and Center for Emerging Material  
and Advanced Devices  
National Taiwan University  
Taipei 106, Taiwan



DOI: 10.1002/aenm.201100581

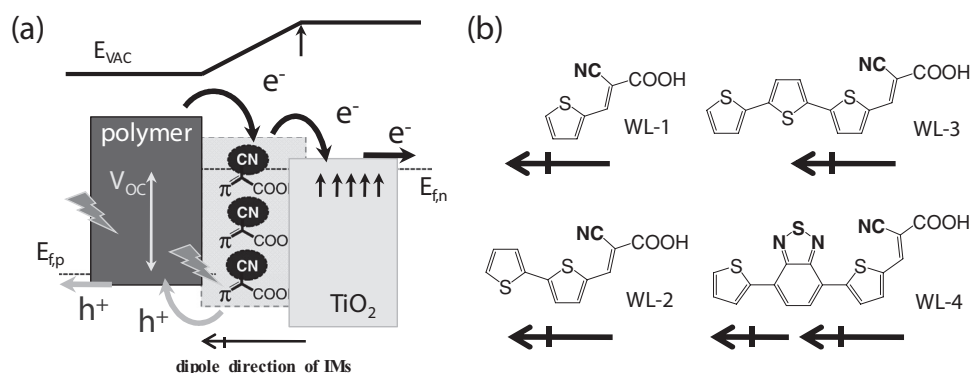


**Figure 1.** a) Energy level diagram of the interface of polymer/interfacial modifiers (IMs)/TiO<sub>2</sub> in a hybrid solar cell. ( $E_{\text{VAC}}$ : vacuum level,  $E_{f,p}$ : quasi-Fermi level of holes,  $E_{f,n}$ : quasi-Fermi level of electrons,  $V_{\text{OC}}$ : open-circuit voltage). b) Chemical structures of IMs (WL-1 to WL-4).

dipole pointing toward substrate downshifts the work function of substrate.<sup>[28]</sup> This phenomenon has been widely exploited to enhance charge injection from metals into organic materials in organic light-emitting diodes and field-effect transistors.<sup>[29,30]</sup> In 2007, based on a series of *para*-substituted benzoic acids as the IMs of P3HT/TiO<sub>2</sub> heterojunction, McGehee and co-workers<sup>[31]</sup> systematically examined the effect of IMs on the photovoltaic properties of hybrid solar cells. According to their results, both molecular dipole of IM and the acid–base interaction between Ti –OH and –COOH moieties can cause a band-edge shift in TiO<sub>2</sub>, subsequently changing the open-circuit voltage ( $V_{\text{OC}}$ ). As expected,  $V_{\text{OC}}$  increases while electron-donating groups, such as –NH<sub>2</sub> and –OCH<sub>3</sub>, substituted benzoic acids are applied as IMs, due to the formation of a molecular dipole directing away from TiO<sub>2</sub> that shifts the band-edge of titania closer to the vacuum level of the polymer, thus increasing the effective gap between the conduction band of TiO<sub>2</sub> and the highest occupied molecular orbital (HOMO) of P3HT. However, these electron-rich substituents diminish the electron affinity of IMs, resulting in a decline in the short-circuit current density ( $J_{\text{SC}}$ ). Both  $V_{\text{OC}}$  and  $J_{\text{SC}}$  could not be improved simultaneously to increase the cell efficiency. Conversely, an electron-withdrawing group substituted benzoic acid increases the  $J_{\text{SC}}$  value, yet decreases the  $V_{\text{OC}}$  value.

In addition, several studies demonstrated the feasibility of increasing the  $J_{\text{SC}}$  value by applying organic or Ru-dyes as the IMs of TiO<sub>2</sub> and polymer.<sup>[32–35]</sup> Such an increase is possible owing to the enhanced light harvesting by dye molecules and the cascaded electron transfer from conjugated polymer, IMs to TiO<sub>2</sub> as the lowest unoccupied molecular orbital (LUMO) of IMs sits in between the LUMO of P3HT and the conduction band of titania. In this study, a class of conjugated cyanoacrylic acids (WL-series, as shown in Figure 1b) was synthesized and then used to improve the interface between P3HT and TiO<sub>2</sub>. An electron-withdrawing moiety was designed on the side of the –COOH anchoring group to produce a molecular dipole pointing away from TiO<sub>2</sub> surface and raise the electron affinity of molecules, especially in the region near TiO<sub>2</sub>. Therefore, as expected, both  $V_{\text{OC}}$  and  $J_{\text{SC}}$  can be increased simultaneously. Moreover, the LUMO of IMs was fine tuned by lengthening the conjugation length or adopting a donor–acceptor structure. These molecules allow us to investigate systematically how the

LUMO position of IMs affects the contribution of P3HT excitons to the photocurrent and cell efficiency.

## 2. Results and Discussion

### 2.1. Design and Synthesis of Interfacial Modifiers

A series of conjugated molecules was synthesized and applied as the surface modifier of TiO<sub>2</sub> to examine how the energy levels and dipole moments of molecules affect the photovoltaic behavior of P3HT/TiO<sub>2</sub> hybrid solar cells. The design strategy of molecular structure includes using cyanoacrylic acid moiety to provide grafting ability and dipoles directing away TiO<sub>2</sub>. Both the LUMO and bandgap were tuned by the increment of the number of thiophene rings and the incorporation of benzothiadiazole as an electron acceptor into the  $\pi$ -conjugated backbone. Figure 1b displays the chemical structure of these molecules. The thiophene end-groups may also improve their compatibility with P3HT.

Figure S1 (Supporting Information) depicts the synthetic routes of IMs, WL-1 to WL-4. Thiophene oligomers and benzothiadiazole derivative were synthesized by Kumada or Stille coupling. The corresponding conjugated precursors were then formylated by Vilsmeier–Haack reaction, followed by treatment with cyanoacetic acid under typical Knoevenagel condensation to produce the target IMs. Their chemical structures were fully characterized with <sup>1</sup>H NMR, <sup>13</sup>C NMR, and EI-MS (as shown in Supporting Information).

### 2.2. Optical and Electrochemical Properties of Interfacial Modifiers

Figure 2a shows the molar absorption spectra of WL-1 to WL-4 IMs dissolved in tetrahydrofuran (THF). A visible absorption band corresponding to the  $\pi$ – $\pi^*$  transition is observed for WL-1 to WL-3. As expected, the absorption maximum ( $\lambda_{\text{max}}$ ) red-shifts from 337 nm ( $\epsilon = 20\,400\text{ M}^{-1}\text{cm}^{-1}$ ), 407 nm ( $\epsilon = 20\,200\text{ M}^{-1}\text{cm}^{-1}$ ) to 444 nm ( $\epsilon = 44\,600\text{ M}^{-1}\text{cm}^{-1}$ ) as the number of thiophene rings along the backbone increases from one to three. Upon incorporation of benzothiadiazole,  $\lambda_{\text{max}}$  is further red-shifted

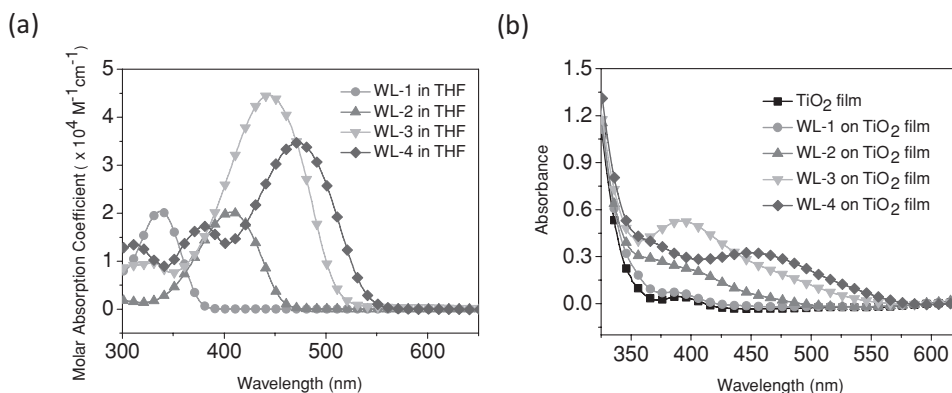


**Figure 2.** UV-vis absorption spectra of WL-1, WL-2, WL-3, and WL-4 a) dissolved in THF and b) adsorbed on a 250 nm thick mesoporous TiO<sub>2</sub> film.

to 472 nm ( $\epsilon = 34\,700\text{ M}^{-1}\text{cm}^{-1}$ ) with two weaker absorption bands appearing at 313 nm ( $\epsilon = 13\,500\text{ M}^{-1}\text{cm}^{-1}$ ) and 381 nm ( $\epsilon = 17\,300\text{ M}^{-1}\text{cm}^{-1}$ ), indicating the donor–acceptor structure shortens the optical bandgap.

The redox properties of WL-series IMs were examined using cyclic voltammetry (CV), in which ferrocene was used as the internal standard. According to Figure S2 (Supporting Information), all cyclic voltammograms exhibit an irreversible oxidation curve with no reduction wave deducted. The HOMO was then calculated from the onset potential of oxidation wave ( $E_{\text{ox,onset}}$ ), according to the formula of  $\text{HOMO} = -[(E_{\text{ox,onset}} - E_{\text{Fc}^+}) + 4.8\text{ eV}]$ , where  $E_{\text{Fc}^+}$  denotes the measured oxidation potential of ferrocene and 4.8 eV is the absolute oxidation potential value of ferrocene under vacuum. Notably,  $E_{\text{ox,onset}}$  of WL-1 to WL-3 decreases with an increasing number of thiophene units, indicating that extending  $\pi$ -conjugated moieties elevates the electropositive over the molecular structure and increases the oxidized ability, ultimately raising HOMO for about 0.7 eV from WL-1 to WL-3. However, the replacement of the central thiophene ring in WL-3 with benzothiadiazole unit slightly lowers its oxidation potential so that WL-4 has a  $E_{\text{ox,onset}}$  in between WL-2 and WL-3. This finding suggests that introducing electron-withdrawing moiety into the oligothiophene system lifts the electron affinity and reduces the oxidized ability over the conjugated structure. Moreover, the LUMO can be estimated from the sum of HOMO and optical bandgap, which was determined from the onset absorption in

UV-vis spectra. **Table 1** summarizes all optical and electrochemical properties of IMs. According to this table, although LUMO systematically decreases as the conjugated backbone lengthens, WL-4 possesses the lowest-lying LUMO and the smallest bandgap.

An attempt was made to further elucidate the geometrical and electronic properties of WL-series by performing the density functional theory (DFT) calculation under B3LYP/6-31g\* basis set through use of the Gaussian 03 program package.<sup>[36]</sup> **Figure 3** illustrates the optimized ground state structure of WL-series. This figure reveals that the thiophene units are coplanar with respect to the cyanoacrylic acid group, implying a strong conjugation across the thiophene-cyanoacrylate groups. In addition, the values of oscillator strengths, HOMOs, and LUMOs of these IMs were also estimated using the time-dependent DFT calculation based on the B3LYP/6-31G\* optimized ground state geometries in the vacuum, as listed in Table 1. The oscillator strength,  $f$ , is calculated to have the largest value at the transition state of HOMO to LUMO, illustrating the fact that the most dominant transition is from HOMO to LUMO. The electron density of HOMO is localized mainly on the thiophene moiety, while that of LUMO is localized on the side of cyanoacrylic acid group. In addition to helping to inject electrons from IMs to TiO<sub>2</sub>, this distribution assists in lowering the recombination rate of separated electrons and holes.<sup>[37,38]</sup> The trend of calculated HOMOs and LUMOs correlates well with the experimental results determined by the CV/UV-vis method.

**Table 1.** Optical and electrochemical properties of interfacial modifiers (IMs).

IMs	$\lambda_{\text{max}}^{\text{a)}$ [nm]	$\epsilon^{\text{a)}$ [ $\text{M}^{-1}\text{cm}^{-1}$ ]	$\lambda_{\text{onset}}^{\text{a)}$ [nm]	$E_{0,0}^{\text{b)}$ [eV]	HOMO <sup>c)/LUMO<sup>d)</sup> [eV]</sup>	$\mu_x^{\text{e)}$ [D]	$\mu_y^{\text{e)}$ [D]	$\mu_z^{\text{e)}$ [D]	$\mu_{\text{total}}^{\text{e)}$ [D]	$f^{\text{e)}$	Transition weight <sup>e)</sup>	HOMO <sup>d)/LUMO<sup>e)</sup> [eV]</sup>
WL-1	337	20,400	379	3.27	-6.16/-2.89	0.00	2.84	3.28	4.34	0.51	60% HOMO → LUMO	-6.90/-3.03
WL-2	407	20,200	470	2.64	-5.74/-3.10	-0.19	2.53	4.29	4.99	0.83	61% HOMO → LUMO	-6.21/-3.12
WL-3	444	44,600	523	2.37	-5.47/-3.10	0.20	3.21	5.35	6.24	1.09	62% HOMO → LUMO	-5.85/-3.15
WL-4	472	34,700	552	2.25	-5.61/-3.36	-0.09	4.83	5.02	6.97	0.71	62% HOMO → LUMO	-5.92/-3.44

$\lambda_{\text{max}}$ : the wavelength of the absorption peak;  $\epsilon$ : absorption coefficient;  $\lambda_{\text{onset}}$ : the onset wavelength of the absorption spectrum;  $E_{0,0}$ : the lowest transition energy;  $\mu$ : dipole moment;  $f$ : oscillator strength for the lowest energy transition (HOMO → LUMO); <sup>a)</sup>Absorptions were measured in THF; <sup>b)</sup> $E_{0,0}$  were determined by onset wavelengths of the corresponding absorption spectra in THF; <sup>c)</sup>The formal oxidation potentials (versus NHE) were internally calibrated with ferrocene and taken as the HOMO; <sup>d)</sup>LUMO was calculated by HOMO +  $E_{0,0}$ ; <sup>e)</sup>Density functional theory/time-dependent density functional theory calculated values (in the vacuum); the Z-axis corresponds to the TiO<sub>2</sub> surface normal; the transition weight is the composition in terms of molecular orbital contributions of the lowest energy transition.

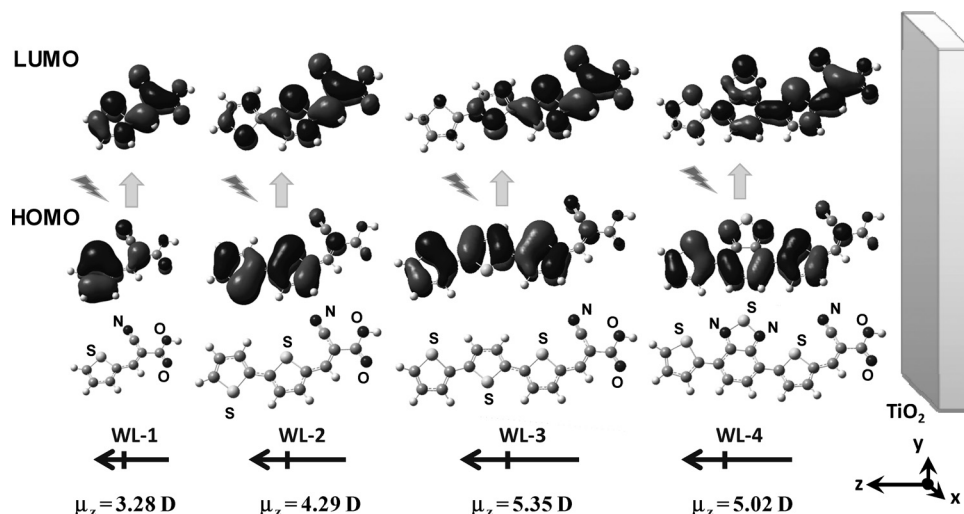


**Figure 3.** The optimized ground state structures, the dipole moments perpendicular to the  $\text{TiO}_2$  surface ( $\mu_z$ ), and the electronic density distributions of highest occupied molecular orbital (HOMO) and lowest unoccupied molecular orbital (LUMO) of WL-series interfacial modifiers.

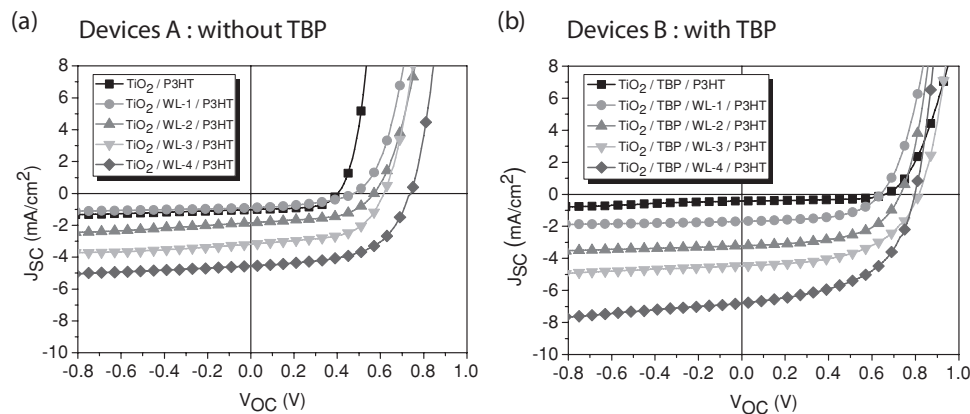
### 2.3. Fabrication and Performance of Photovoltaic Devices

Figure S3 (Supporting Information) shows the schematic structure and scanning electron microscopy (SEM) images of solar devices. Rough fluorine-doped tin oxide (FTO) with distinct crystallites was fully covered with a thin layer of dense  $\text{TiO}_2$  to prevent the direct contact of P3HT with FTO electrode. The mesoporous  $\text{TiO}_2$  layer was made by the dip-coating procedure from an ethanol solution comprising  $(\text{TiOEt})_4$  precursor and an amphiphilic triblock copolymer, Pluronic P123, which functions as a structure directing agent. Mesopores were formed by calcinating the hybrid film at  $450^\circ\text{C}$  to burn out the copolymer.<sup>[39]</sup> Figure S3 indicates that the as-prepared porous film has pore sizes of 8–10 nm and a thickness of around 230–250 nm.

This study also attempted to improve the compatibility of P3HT and  $\text{TiO}_2$  by modifying the titania surface with a layer of IMs. Figure 2b displays the UV-vis spectra of WL-1 to WL-4 adsorbed on a 250 nm thick  $\text{TiO}_2$  films. Compared to the solution spectra of corresponding IMs, they exhibit an evident

blue-shift. Next,  $\lambda_{\text{max}}$  of WL-3 on  $\text{TiO}_2$  film is blue-shifted by 52 nm from 444 nm of its THF solution, while that of WL-4 is shifted by 23 nm from 472 nm. This is mainly owing to either the acid–base interactions of  $-\text{COOH}$  and  $\text{TiO}_2$  or the formation of H-aggregates of IMs on  $\text{TiO}_2$  surface.<sup>[40]</sup> The electron-withdrawing moiety of benzothiadiazole in WL-4 apparently renders a stronger molecular dipole that counterbalanced the deprotonation effect of IMs, resulting in a smaller blue shift in  $\lambda_{\text{max}}$  for WL-4 compared to WL-3 upon anchoring onto  $\text{TiO}_2$ .<sup>[41]</sup> Moreover, 4-*tert*-butyl-pyridine (TBP) was employed to physically plug the surface voids at molecular scale and take advantage of its basicity to reduce the protonation effect of  $\text{TiO}_2$ .<sup>[31,35,42]</sup> After infiltrating P3HT into the mesopores of  $\text{TiO}_2$  layer by heat treatment,<sup>[39]</sup> Au (5 nm) and Ag (100 nm) were subsequently deposited on top of P3HT to serve as the back electrode and increase the light reflectivity inside the device.<sup>[43]</sup>

Figure 4 displays the current density–voltage curves of devices with bare or various IMs-modified  $\text{TiO}_2$ , under A.M. 1.5G



**Figure 4.** Current–voltage curves of solar devices fabricated from P3HT/interfacial modifiers (WL-1 to WL-4)/ $\text{TiO}_2$  a) without TBP treatment (devices A) and b) with TBP treatment (devices B), which were measured under A.M. 1.5G simulated illumination at  $100\text{ mW cm}^{-2}$ .

**Table 2.** Photovoltaic characteristics of solar cells fabricated from P3HT/interfacial modifiers (WL-1 to WL-4)/TiO<sub>2</sub> without (devices A) and with (devices B) TBP treatment, which were measured under A.M. 1.5G simulated illumination at 100 mW cm<sup>-2</sup>.

Devices A IMs	V <sub>OC</sub> [V]	J <sub>SC</sub> [mA cm <sup>-2</sup> ]	FF [%]	η [%]	R <sub>s</sub> [Ωcm <sup>2</sup> ]	R <sub>sh</sub> [kΩcm <sup>2</sup> ]	Devices B IMs	V <sub>OC</sub> [V]	J <sub>SC</sub> [mA cm <sup>-2</sup> ]	FF [%]	η [%]	R <sub>s</sub> [Ωcm <sup>2</sup> ]	R <sub>sh</sub> [kΩcm <sup>2</sup> ]
/	0.41	1.03	57.58	0.24	2.19	2.02	TBP	0.65	0.60	51.96	0.20	8.42	5.24
WL-1	0.48	0.89	41.78	0.18	6.94	2.10	WL-1/TBP	0.65	1.69	54.16	0.59	10.07	2.47
WL-2	0.58	1.84	53.46	0.57	7.99	1.17	WL-2/TBP	0.74	3.21	54.50	1.30	7.26	1.83
WL-3	0.62	3.18	56.36	1.11	6.31	0.92	WL-3/TBP	0.82	4.46	52.82	1.93	9.27	1.71
WL-4	0.75	4.54	55.70	1.90	5.73	1.23	WL-4/TBP	0.80	6.79	52.81	2.87	6.11	0.74

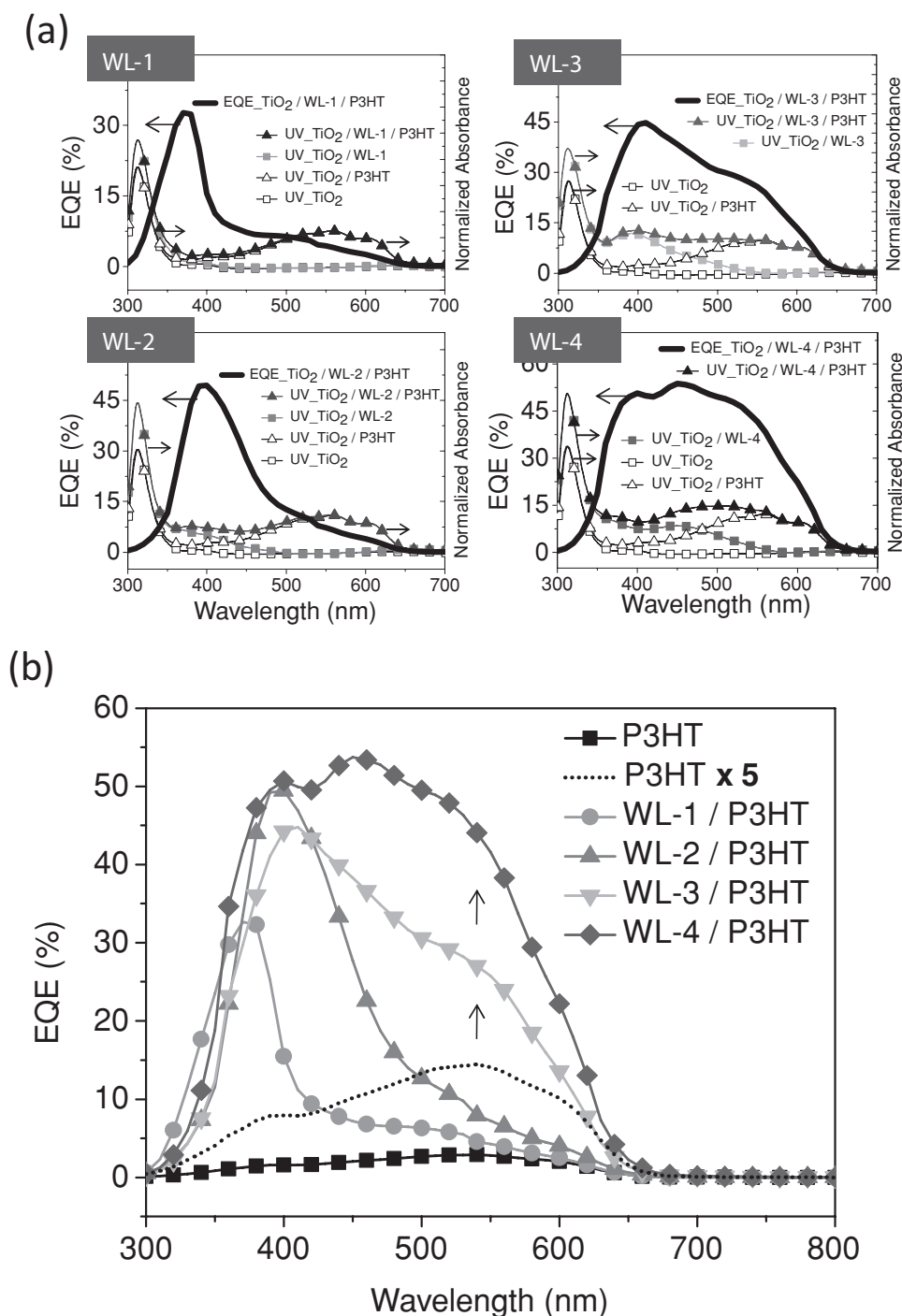
simulated illumination at 100 mW/cm<sup>2</sup>. As presented in **Table 2**, all devices with IMs-modified TiO<sub>2</sub> have a higher V<sub>OC</sub> than the one with unmodified TiO<sub>2</sub> and the V<sub>OC</sub> of A-series devices, in which no TBP is used, increases in the order of WL-1, WL-2, WL-3, and WL-4. It has been demonstrated that the maximum value of V<sub>OC</sub> is strongly associated with the band edge difference between the conduction band (E<sub>CB</sub>) of TiO<sub>2</sub> and the HOMO level (E<sub>HOMO</sub>) of polymer. As is well known, self-assembly of IMs on titania that produces a thin layer of dipoles pointing away from the TiO<sub>2</sub> surface, shifts the band edge potential of TiO<sub>2</sub> upward, consequently raising the E<sub>CB</sub>-E<sub>HOMO</sub> gap and the achievable V<sub>OC</sub>.<sup>[28,31,44]</sup> On the other hand, the carboxylic acid group of IMs may protonate the titania surface to yield dipoles pointing toward TiO<sub>2</sub>, which counteracts the upward shift of TiO<sub>2</sub> conduction band edge.<sup>[31,45,46]</sup> Upon treating TiO<sub>2</sub> with TBP, B-series devices, V<sub>OC</sub> increases significantly, suggesting that TBP effectively reduces the unfavorable protonation effect of titania. Moreover, the B-series devices generally have a higher shunt resistance (R<sub>sh</sub>) than that of A-series devices, revealing that the co-adsorption of TBP on TiO<sub>2</sub> could also retard the charge recombination in P3HT/TiO<sub>2</sub> interface.<sup>[47]</sup> Interestingly, in contrast with A-series devices, the device with WL-3 has the highest V<sub>OC</sub> in B-series devices. To quantitatively correlate IM's dipole moment with the V<sub>OC</sub> of P3HT/TiO<sub>2</sub> cells, the intrinsic dipole moment (μ<sub>total</sub>) of IMs in the gas phase was determined by the DFT approach and listed in Table 1. It shows the μ<sub>total</sub> increases as the number of donor moieties increases or as an electron acceptor unit, benzothiadiazole, is inserted in between two thiophene rings. Figure 3 reveals that these IMs are somewhat adsorbed perpendicularly on TiO<sub>2</sub> surface. Therefore, the μ<sub>total</sub> vector was decomposed into three components along the x-, y-, and z-axes, where μ<sub>z</sub> represents the dipole moment along the molecular backbone. This finding clearly reveals that WL-3 has the highest μ<sub>z</sub> among the four IMs studied. Also, the order of the μ<sub>z</sub> value coincides perfectly with the order of measured V<sub>OC</sub>'s.

Table 2 clearly indicates that treating TiO<sub>2</sub> with IMs markedly increases the J<sub>SC</sub> value of devices. Moreover, the B-series devices exhibit a higher J<sub>SC</sub> than that of the corresponding cells of A-series, except the one without IMs. A previous study has established that TBP molecules can plug the voids of dye-covered TiO<sub>2</sub> surface and insulate the aggregation of dyes that retards charge recombination as well as facilitates more exciton dissociation and charge injection at the heterojunction interface, further elevating the J<sub>SC</sub> value. For devices based on bare TiO<sub>2</sub>, the presence of TBP may lower the efficiency of photoexcited

electron injection from P3HT to TiO<sub>2</sub> due to the higher-lying LUMO of TBP than that of P3HT.

**Figure 5a** shows the UV-vis spectra of active components and the corresponding external quantum efficiency (EQE) spectra of TBP-treated devices that consist of various IMs-modified TiO<sub>2</sub>. A noticeable difference is observed in the shape of the EQE spectra. Although the absorption of IMs dominates the contribution of photocurrent for those devices based on WL-1 and WL-2, the role of P3HT becomes visible as WL-3 and WL-4 are used. These findings evidently indicate not only that excitons generated by the light harvest of both P3HT and IMs contribute to the photocurrent, but also that the type of IMs profoundly impacts the efficiency of transferring excited electrons from P3HT to TiO<sub>2</sub>.

This study more closely examined how the IMs affect the contribution ratio of photocurrent from both sources. **Figure 5b** replots all EQE spectra. The onset absorption (λ<sub>onset</sub>) of all IMs used in this study is shorter than 570 nm, and P3HT has absorption maxima at around 530–570 nm. Therefore, the EQE at 570 nm is assumed to be almost exclusively ascribed to P3HT. Without IMs, the solar device has an extremely low EQE of below 3% with a maximum at 540 nm, indicating that the photon-to-electron converting ability of P3HT/bare TiO<sub>2</sub> is inefficient. Interestingly, the type of IMs has significant impact on the quantity of P3HT-generated photocurrent. The EQE at 570 nm increases progressively from 3.6% of WL-1, 5.7% of WL-2, 21.3% of WL-3, to 33.8% of WL-4. For this device type, the excited electron created in P3HT should traverse IMs to inject into the conduction band of TiO<sub>2</sub>. Therefore, the LUMO position of IMs may affect the injection efficiency of P3HT excitons, as depicted in **Figure 6**. Although the E<sub>LUMO</sub> of WL-1 (-2.89 eV) is higher lying than that of P3HT (≈-3.0 eV), the EQE of TiO<sub>2</sub>/WL-1/P3HT at 570 nm is still roughly 1.5 times higher than that of TiO<sub>2</sub>/P3HT. This observation implies that the electron-withdrawing group of cyanoacrylic acid in WL-1 may elevate the electron affinity near TiO<sub>2</sub> surface, and the thiophene end group may also enhance the interfacial compatibility between P3HT and TiO<sub>2</sub>. In contrast, the LUMO levels of WL-2 to WL-4 lie between the E<sub>LUMO</sub> of P3HT and the E<sub>CB</sub> of TiO<sub>2</sub>, thus facilitating a cascade of electron migration from P3HT to TiO<sub>2</sub> via IMs. As the LUMO of the IMs downshifts from -3.10 to -3.36 eV, J<sub>SC</sub> increases from 3.21 to 6.79 mA cm<sup>-2</sup>, accompanied by an increase in the contribution of P3HT to EQE. This finding demonstrates that a larger energy offset benefits the efficient exciton dissociation and charge injection. To the best



**Figure 5.** a) External quantum efficiency (EQE) spectra of WL-1, WL-2, WL-3, and WL-4 modified P3HT/TiO<sub>2</sub> hybrid solar devices and normalized UV-vis absorption spectra of corresponding films; b) EQE spectra of P3HT/TiO<sub>2</sub> hybrid solar cells with bare or various interfacial modifiers (IMs), WL-1 to WL-4, treated TiO<sub>2</sub>.

of the authors' knowledge, this is the first investigation to optimize systematically the EQE of P3HT by fine-tuning the LUMO level of IMs. Accordingly, the WL-4-modified cell exhibits the highest power conversion efficiency of 2.87% with a  $V_{OC}$  of 0.8 V, a  $J_{SC}$  of 6.79 mA cm<sup>-2</sup> and an FF of 52.81%.

### 3. Conclusions

The interface of the P3HT/TiO<sub>2</sub> heterojunction in hybrid solar cells was modified using conjugated cyanoacrylic acid derivatives. The thiophene end-groups in the IMs apparently improve

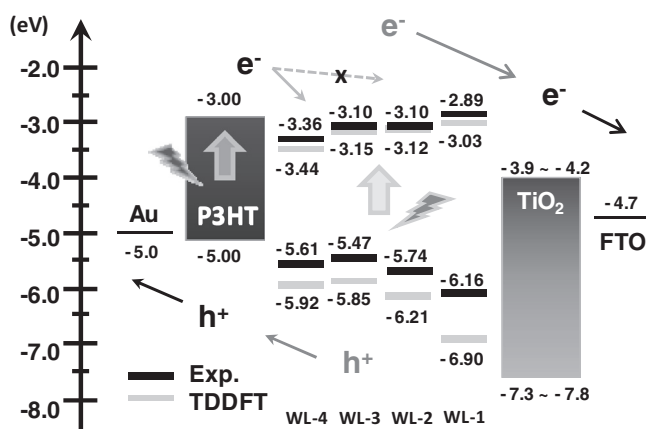


**Figure 6.** Energy level diagrams and charge transfer processes of solar devices fabricated from P3HT/IMs/TiO<sub>2</sub>, where Exp. denotes the energy levels, which were experimentally determined from UV-vis spectrum and cyclic voltamogram; TDDFT denotes the calculated values using time-dependent density functional theory.

the mutual compatibility of P3HT and TiO<sub>2</sub>. Incorporating a strong electron-withdrawing –CN moiety adjacent to the –COOH anchoring group in the molecular structure of the IMs induces a molecular dipole directing away from the titania surface, and enhances the electron affinity of the molecules, simultaneously increasing the  $J_{SC}$  and  $V_{OC}$  of the device. The increment in  $V_{OC}$  is consistent with the order of the dipole moment along the molecular backbone of the IM. EQE spectra clearly indicate that excitons that are generated in both IMs and P3HT make contribution to  $J_{SC}$ . All IMs herein considerably increase the EQE at 570 nm, which is attributed to the light harvesting of P3HT, although WL-1 has a LUMO that is slightly higher than that of P3HT, suggesting the IMs greatly improve the P3HT/TiO<sub>2</sub> interface, promoting the dissociation of P3HT excitons. Furthermore, the LUMO of IMs plays an important role in determining the efficiency of the injection of electrons from P3HT to TiO<sub>2</sub>. The order of EQE at 570 nm (WL-4 > WL-3 > WL-2), which represents the degree of contribution of P3HT, coincides perfectly with the order of the LUMO offset of IMs and P3HT, revealing that an energy offset of greater than ≈0.3 eV between the LUMOs of P3HT and the IM promotes the smooth electron injection from P3HT through IM to TiO<sub>2</sub>. This study provides valuable guidelines for further designing novel IMs for use in the development of high-efficiency polymer/inorganic hybrid solar cells and solid-state dye-sensitized solar cells.

#### 4. Experimental Section

**Synthesis and Characterization of Interfacial Modifiers:** Four IMs of WL-1 to WL-4 were synthesized by the preparation of corresponding conjugated precursors with Kumada or Stille coupling methods, followed by performing Vilsmeier–Haack reaction and then Knoevenagel condensation. The detailed synthesis procedures and characterization data are provided in Supporting Information.

**Fabrication of Hybrid Photovoltaic Devices:** The fluorine-doped SnO<sub>2</sub> (FTO, 15 Ω<sup>-2</sup>) substrates were ultrasonically cleaned with detergent, deionized water, acetone, and isopropyl alcohol and then dried in N<sub>2</sub>

flow. A precursor solution of titanium isopropoxide–acetylacetonate complexes was prepared by mixing titanium isopropoxide (0.284 g) with acetylacetonate (0.203 g) in ethanol (5.0 mL). The solution was deposited by the spray pyrolysis method using N<sub>2</sub> as carrying gas at a flow rate of 400 c.c. min<sup>-1</sup>, on a cleaned FTO glass surface preheated to 450 °C. Following deposition, films were calcined under air for 5 min at 450 °C, yielding dense TiO<sub>2</sub> films with a thickness of around 50–60 nm. Mesoporous TiO<sub>2</sub> films were then prepared by adding a solution containing concentrated HCl (3.205 g) and titanium ethoxide (4.302 g) to Pluronic P123 triblock copolymer (1.007 g) dissolved in ethanol (15.0 mL). After 3–4 h of vigorously stirring at room temperature, the resulting solution was dip-coated on top of FTO/dense TiO<sub>2</sub> substrates at a speed of 6 cm min<sup>-1</sup>, followed by rapid thermal treatment at 450 °C for 5 min and then gradually cooled to ambient temperature. The above dip-coating process was repeated one more time to yield a porous TiO<sub>2</sub> layer with a thickness of 230–250 nm. Next, the mesoporous film was calcined at 500 °C for 4 h. After the subsequently prepared substrates had cooled to 80 °C, they were immersed into WL-series IMs solution (1.0 × 10<sup>-3</sup> M) prepared in anhydrous THF overnight, followed by rinsing in THF three times and drying in N<sub>2</sub> flow. P3HT solution (15.0 mg mL<sup>-1</sup>, dissolved in a solvent mixture of *o*-dichlorobenzene and chlorobenzene with a volume ratio of 3:1), was spin-coated on top of the IM-modified TiO<sub>2</sub> layer (1000 rpm for 30 s), and then heated at 125 °C for 7 min to facilitate the filtration of P3HT into titania pores. For samples with TBP treatment, the IM-modified TiO<sub>2</sub> films were spin-coated with a TBP solution (0.05 M) in *p*-xylene (3500 rpm for 30 s), and dried in N<sub>2</sub> flow prior to depositing P3HT layer. Finally, the devices were coated with Au (5 nm) and Ag (100 nm) by an evaporation route under vacuum (lower than 1 × 10<sup>-5</sup> Torr) in an EDWARDS AUTO 306 vacuum evaporation system.

**Characterization:** The <sup>1</sup>H NMR and <sup>13</sup>C NMR spectra were collected on BRUKER AC-300 and AC-400 MHz spectrometers, respectively. All NMR spectra were calibrated by D-chloroform (CDCl<sub>3</sub>) or dimethyl sulfoxide D6 (DMSO-d<sub>6</sub>) signal, where <sup>1</sup>H NMR chemical shifts of CDCl<sub>3</sub> and DMSO-d<sub>6</sub> are 7.24 ppm and 2.50 ppm, respectively; in addition, <sup>13</sup>C NMR of DMSO-d<sub>6</sub> is 39.5 ppm. The peak multiplicity was described as follows: s = singlet, d = doublet, t = triplet, q = quartet, p = pentet, dd = doublets of doublets, and m = multiplet. Low resolution electron ionization mass spectra (MS/EI) were collected using a Finnigan TSQ 700. Optical absorbance measurements were taken by a JASCO V-670 UV/Vis spectrophotometer. The UV/Vis spectra of IMs in 2.5 × 10<sup>-5</sup> M solution of THF were measured in a range of 300–700 nm, while the solid state UV/Vis spectra of FTO/TiO<sub>2</sub>/IMs and FTO/TiO<sub>2</sub>/IMs/P3HT were measured in a range of 300–800 nm. CV of all IMs were analyzed using CH Instruments model of CHI 660A with three electrode cells in anhydrous DMF solution containing 0.1 M tetra-*n*-butylammonium hexafluorophosphate at a scan rate of 30 mV s<sup>-1</sup> under N<sub>2</sub> atmosphere. The three electrodes used in the CV measurement were as follows: (i) glassy carbon as the working electrode, (ii) platinum as the counter electrode, and (iii) saturated aqueous Ag/AgCl as the reference electrode. The reference electrode was calibrated by running the CV of ferrocene without adding IM to the solution. The morphology and thickness of dense and mesoporous TiO<sub>2</sub> films were examined using a field-emission scanning electron microscope (JSM-6700F, JEOL Company). The current density–voltage (*J*–*V*) characteristics of photovoltaic devices were evaluated with a Keithley 2400 source meter under AM 1.5G solar irradiation obtained from a 300 W Oriel solar simulator, at 100 mW cm<sup>-2</sup>, which was calibrated by a mono-Si reference cell with a KG5 filter. The EQE spectra were recorded under illumination by a xenon lamp and a monochromator (TRIAx 180, JOBIN YVON), and the light intensity was calibrated by using an OPHIR 2A-SH thermopile detector.

#### Supporting Information

Supporting Information is available from the Wiley Online Library or from the author.

## ACKNOWLEDGEMENTS

The authors thank National Taiwan University, Academia Sinica, and the National Science Council of the Republic of China (NSC 100-3113-E-008-003) for financially supporting this research. We are grateful to the National Center for High-Performance Computing for computer time and facilities. We also would like to acknowledge the Valued Instruments Center of National Taiwan Normal University for NMR experiments and the Instrumentation Center of National Taiwan University for SEM and EI-MS experiments.

Received: September 27, 2011

Revised: November 2, 2011

Published online: November 25, 2011

- [1] G. Yu, J. Gao, J. C. Hummelen, F. Wudi, A. J. Heeger, *Science* **1995**, *270*, 1789.
- [2] J. Weickert, R. B. Dunbar, H. C. Hesse, W. Wiedemann, L. Schmidt-Mende, *Adv. Mater.* **2011**, *23*, 1810.
- [3] A. C. Arias, *Chem. Rev.* **2010**, *110*, 3.
- [4] B. C. Thompson, J. M. J. Fréchet, *Angew. Chem. Int. Ed.* **2008**, *47*, 58.
- [5] Y.-J. Cheng, C.-H. Hsieh, Y. He, C.-S. Hsu, Y. Li, *J. Am. Chem. Soc.* **2010**, *132*, 17381.
- [6] H. Zhou, L. Yang, A. C. Stuart, S. C. Price, S. Liu, W. You, *Angew. Chem. Int. Ed.* **2011**, *50*, 2995.
- [7] H.-Y. Chen, J. Hou, S. Zhang, Y. Liang, G. Yang, Y. Yang, L. Yu, Y. Wu, G. Li, *Nat. Photonics* **2009**, *3*, 649.
- [8] M. D. Heinemann, K. von Maydell, F. Zutz, J. Kolny-Olesiak, H. Borchert, I. Riedel, J. Parisi, *Adv. Funct. Mater.* **2009**, *19*, 3788.
- [9] S. Dayal, M. O. Reese, A. J. Ferguson, D. S. Ginley, G. Rumbles, N. Kopidakis, *Adv. Funct. Mater.* **2010**, *20*, 2629.
- [10] N. Radychev, I. Lokteva, F. Witt, J. Kolny-Olesiak, H. Borchert, J. Parisi, *J. Phys. Chem. C* **2011**, *115*, 14111.
- [11] K.-J. Jiang, K. Manseki, Y.-H. Yu, N. Masaki, K. Suzuki, Y.-I. Song, S. Yanagida, *Adv. Funct. Mater.* **2009**, *19*, 2481.
- [12] A. Abrusci, R. S. S. Kumar, M. Al-Hashimi, M. Heeney, A. Petrozza, H. J. Snaith, *Adv. Funct. Mater.* **2011**, *21*, 2571.
- [13] J. A. Chang, J. H. Rhee, S. H. Im, Y. H. Lee, H.-J. Kim, S. I. Seok, M. K. Nazeeruddin, M. Grätzel, *Nano Lett.* **2010**, *10*, 2609.
- [14] S. D. Oosterhout, L. J. A. Koster, S. S. van Bavel, J. Loos, O. Stenzel, R. Thiedmann, V. Schmidt, B. Campo, T. J. Cleij, L. Lutzen, D. Vanderzande, M. M. Wienk, R. A. J. Janssen, *Adv. Energy Mater.* **2011**, *1*, 90.
- [15] X. Bulliard, S.-G. Ihn, S. Yun, Y. Kim, D. Choi, J.-Y. Choi, M. Kim, M. Sim, J.-H. Park, W. Choi, K. Cho, *Adv. Funct. Mater.* **2010**, *20*, 4381.
- [16] T. Xu, Q. Qiao, *Energy Environ. Sci.* **2011**, *4*, 2700.
- [17] J. Bouclé, P. Ravirajan, J. Nelson, *J. Mater. Chem.* **2007**, *17*, 3141.
- [18] T. R. B. Foong, Y. Shen, X. Hu, A. Sellinger, *Adv. Funct. Mater.* **2010**, *20*, 1390.
- [19] W.-C. Yen, Y.-H. Lee, J.-F. Lin, C.-A. Dai, U.-S. Jeng, W.-F. Su, *Langmuir* **2011**, *27*, 109.
- [20] Y.-C. Huang, J.-H. Hsu, Y.-C. Liao, W.-C. Yen, S.-S. Li, S.-T. Lin, C.-W. Chen, W.-F. Su, *J. Mater. Chem.* **2011**, *21*, 4450.
- [21] J. Weickert, F. Auras, T. Bein, L. Schmidt-Mende, *J. Phys. Chem. C* **2011**, *115*, 15081.
- [22] Y.-Y. Lin, T.-H. Chu, S.-S. Li, C.-H. Chuang, C.-H. Chang, W.-F. Su, C.-P. Chang, M.-W. Chu, C.-W. Chen, *J. Am. Chem. Soc.* **2009**, *131*, 3644.
- [23] R. A. Krüger, T. J. Gordon, T. Baumgartner, T. C. Sutherland, *ACS Appl. Mater. Interfaces* **2011**, *3*, 2031.
- [24] B. D. Boer, A. Hadipour, M. M. Mandoc, T. van Woudenberg, P. W. M. Blom, *Adv. Mater.* **2005**, *17*, 621.
- [25] G. Heimel, L. Romaner, E. Zojer, J.-L. Brédas, *Nano Lett.* **2007**, *7*, 932.
- [26] H. Ishii, K. Sugiyama, E. Ito, K. Seki, *Adv. Mater.* **1999**, *11*, 605.
- [27] S. Braun, W. R. Salaneck, M. Fahlman, *Adv. Mater.* **2009**, *21*, 1450.
- [28] J. Krüger, U. Bach, M. Grätzel, *Adv. Mater.* **2000**, *12*, 447.
- [29] G. Ashkenasy, D. Cahen, R. Cohen, A. Shanzer, A. Vilan, *Acc. Chem. Res.* **2002**, *35*, 121.
- [30] J. S. Park, B. R. Lee, J. M. Lee, J.-S. Kim, S. O. Kim, M. H. Song, *Appl. Phys. Lett.* **2010**, *96*, 243306.
- [31] C. Goh, S. R. Scully, M. D. McGehee, *J. Appl. Phys.* **2007**, *101*, 114503.
- [32] R. Zhu, C.-Y. Jiang, B. Liu, S. Ramakrishna, *Adv. Mater.* **2009**, *21*, 994.
- [33] S.-J. Moon, E. Baranoff, S. M. Zakeeruddin, C.-Y. Yeh, E. W.-G. Diau, M. Grätzel, K. Sivula, *Chem. Commun.* **2011**, *47*, 8244.
- [34] W. Zhang, R. Zhu, F. Li, Q. Wang, B. Liu, *J. Phys. Chem. C* **2011**, *115*, 7038.
- [35] G. K. Mor, S. Kim, M. Paulose, O. K. Varghese, K. Shankar, J. Basham, C. A. Grimes, *Nano Lett.* **2009**, *9*, 4250.
- [36] M. J. Frisch, G. W. Trucks, H. B. Schlegel, G. E. Scuseria, M. A. Robb, J. R. Cheeseman, J. A. Montgomery Jr., T. Vreven, K. N. Kudin, J. C. Burant, J. M. Millam, S. S. Iyengar, J. Tomasi, V. Barone, B. Mennucci, M. Cossi, G. Scalmani, N. Rega, G. A. Petersson, H. Nakatsuji, M. Hada, M. Ehara, K. Toyota, R. Fukuda, J. Hasegawa, M. Ishida, T. Nakajima, Y. Honda, O. Kitao, H. Nakai, M. Klene, X. Li, J. E. Knox, H. P. Hratchian, J. B. Cross, V. Bakken, C. Adamo, J. Jaramillo, R. Gomperts, R. E. Stratmann, O. Yazyev, A. J. Austin, R. Cammi, C. Pomelli, J. W. Ochterski, P. Y. Ayala, K. Morokuma, G. A. Voth, P. S. Alvarado, J. J. Dannenberg, V. G. Zakrzewski, S. Dapprich, A. D. Daniels, M. C. Strain, O. Farkas, D. K. Malick, A. D. Rabuck, K. Raghavachari, J. B. Foresman, J. V. Ortiz, Q. Cui, A. G. Baboul, S. Clifford, J. Cioslowski, B. B. Stefanov, G. Liu, A. Liashenko, P. Piskorz, I. Komaromi, R. L. Martin, D. J. Fox, T. Keith, M. A. Al-Laham, C. Y. Peng, A. Nanayakkara, M. Challacombe, P. M. W. Gill, B. Johnson, W. Chen, M. W. Wong, C. Gonzalez, J. A. Pople, *Gaussian 03, Revision B.05*, Gaussian, Inc, Wallingford, CT **2004**.
- [37] D. Shi, Y. Cao, N. Postrakulchote, Z. Yi, M. Xu, S. M. Zakeeruddin, M. Grätzel, P. Wang, *J. Phys. Chem. C* **2008**, *112*, 17478.
- [38] J. Wiberg, T. Marinado, D. P. Hagberg, L. Sun, A. Hagfeldt, B. Albinsson, *J. Phys. Chem. C* **2009**, *113*, 3881.
- [39] K. M. Coakley, Y. Liu, M. D. McGehee, K. L. Frindell, G. D. Stucky, *Adv. Funct. Mater.* **2003**, *13*, 301.
- [40] M. K. R. Fischer, S. Wenger, M. Wang, A. Mishra, S. M. Zakeeruddin, M. Grätzel, P. Bäuerle, *Chem. Mater.* **2010**, *22*, 1836.
- [41] W. Zhu, Y. Wu, S. Wang, W. Li, X. Li, J. Chen, Z.-S. Wang, H. Tian, *Adv. Funct. Mater.* **2011**, *21*, 756.
- [42] S. Yu, S. Ahmadi, C. Sun, P. Palmgren, F. Hennes, M. Zuleta, M. Göthelid, *J. Phys. Chem. C* **2010**, *114*, 2315.
- [43] H. J. Snaith, A. J. Moule, C. Klein, K. Meerholz, R. H. Friend, M. Grätzel, *Nano Lett.* **2007**, *7*, 3372.
- [44] P. Chen, J. H. Yum, F. D. Angelis, E. Mosconi, S. Fantacci, S.-J. Moon, R. Humphry-Baker, J. Ko, M. K. Nazeeruddin, M. Grätzel, *Nano Lett.* **2009**, *9*, 2487.
- [45] Y. Liu, S. R. Scully, M. D. McGehee, J. Liu, C. K. Luscombe, J. M. J. Fréchet, S. E. Shaheen, D. S. Ginley, *J. Phys. Chem. B* **2006**, *110*, 3257.
- [46] S. Meng, E. Kaxiras, *Nano Lett.* **2010**, *10*, 1238.
- [47] S. A. Haque, Y. Tachibana, R. L. Willis, J. E. Moser, M. Grätzel, D. R. Klug, J. R. Durrant, *J. Phys. Chem. B* **2000**, *104*, 538.